Analytical and Bioanalytical Chemistry (2024) 416:5133–5144
https://doi.org/10.1007/s00216-024-05450-2

RESEARCH PAPER

Evaluation of atmospheric-plasma-source absorption mode Fourier transform Orbitrap mass spectrometry for chlorinated paraffin mixtures

Claudia Masucci[1,2] · Konstantin O. Nagornov[3] · Anton N. Kozhinov[3] · Kevin Kraft[1,2] · Yury O. Tsybin[3] · Davide Bleiner[1,2]

Received: 22 April 2024 / Revised: 8 July 2024 / Accepted: 9 July 2024 / Published online: 13 August 2024

Abstract

Chlorinated paraffins (CP) are complex molecular mixtures occurring in a wide range of isomers and homologs of environmental hazards, whose analytical complexity demand advanced mass spectrometry (MS) methods for their characterization. The reported formation of chlorinated olefins (COs) and other transformation products during CP biotransformation and degradation can alter the MS analysis, increasing the high resolution required to distinguish CPs from their degradation products. An advanced setup hyphenating a plasma ionization source and an external high-performance data acquisition and processing system to the legacy hybrid LTQ Orbitrap XL mass spectrometer is reported. First, the study demonstrated the versatility of a liquid sampling atmospheric pressure glow discharge, as a soft ionization technique, for CP analysis. Second, enhanced resolution and sensitivity provided by the absorption mode Fourier transform spectral representation on this legacy mass spectrometer are shown. The developed Orbitrap-based platform allowed the detection of new isotopic clusters and CPs and COs to be distinguished at medium resolution (setting 30,000 at *m*/*z* 400, ~ 400 ms transients), and even chlorinated di-olefins (CdiOs) at higher resolution (setting 100,000 at *m*/*z* 400, ~ 1500 ms transients). Overall, such proof-of-principle instrumental improvements are promising for environmental and analytical research in the field of CP analysis.

Keywords Plasma · FTMS · Mass spectrometry · FTMS Booster · Resolution · LS-APGD

Introduction

Chlorinated paraffins (CP) are a vast group of synthetic compounds widely employed in industrial applications, such as lubricants, plasticizers, and flame-retardants, to name a few [1]. More than one million tons of CP are produced annually by radical chlorination of the respective n-alkanes [2]. The CP have a general molecular formula ($C_nH_{2n+2-x}Cl_x$) characterized by a wide range of carbon chain lengths and different chlorination degrees. Overall, CP consist of various C homologs and Cl homologs (Cl_{2-20}), making the samples complex mixtures [1, 3–5]. CP have been detected in various environmental matrices such as air, water, soil, and sediment, as well as in biota, including fish, birds, and marine mammals [6–14]. Short-chain CP (C_{10-13}) are classified as toxic [15].

State-of-the-art analysis of CP employs mass spectrometry (MS) coupled with gas chromatography (GC) via electron-capture negative ionization (ECNI) or liquid chromatography (LC) coupled with soft ionization techniques such as electrospray or atmospheric pressure chemical ionization (ESI and APCI) [15–19]. Ayala-Cabrera et al. have applied atmospheric pressure photo-ionization (APPI) in a combination with GC–MS to determine and quantify short-chain CP in fish samples, utilizing the selective formation of $[M+Cl]^-$ ions and an internal normalization [20]. Nevertheless, quantification remains a major challenge, if all the species are not known (qualitative information) and reference standard materials are not available.

✉ Davide Bleiner
davide.bleiner@empa.ch

1 Swiss Federal Laboratories for Materials Science and Technology, Überlandstrasse 129, 8600 Dübendorf, Switzerland

2 Department of Chemistry, University of Zürich, Winterthurerstrasse 190, 8057 Zurich, Switzerland

3 Spectroswiss, 1015 Lausanne, Switzerland

In recent years, a simplification trend toward MS analysis with a direct sample injection (infusion) has been observed [21]. Nevertheless, the complex nature of CP mixtures presents an analytical obstacle [7]. Difficulties are prominent when different instrument types or quantification methods are utilized. For instance, ECNI, which is the predominant ionization technique employed for CP analysis, can be influenced by co-eluting compounds or degradation products. The intense fragmentation observed in electron ionization (EI)-MS(/MS) limits its utility to generic CP analysis, lacking the capacity to differentiate CP groups or homologs. In addition, MS may overestimate the degree of chlorination in higher chlorinated CP due to an increased ionization efficiency [10, 22, 23]. Furthermore, CP are usually found together with their transformation products, such as chlorinated olefins (COs) and chlorinated di-olefins (CdiOs), strongly interfering with their detection. The high-resolution MS (HRMS) is needed to resolve the isotopic distributions of CP and CO compounds that overlap due to the minor mass differences between the chlorine and carbon isotopes. For example, the monoisotopic peak of a CP compound $C_{18}H_{32}Cl_6$ and the second isotopologue of a CO compound $C_{18}H_{30}Cl_6$ differ by ~ 18 mDa at *m/z* 458 (if detected as radical anions) requiring resolution exceeding 40,000 to baseline resolve these two peaks.

To overcome these issues, there have been advancements in ionization sources as well as data capturing. For the former, cold plasma-based sources are emerging as soft, flexible, and sensitive solutions which require thorough investigation to understand the underlying chemistry. Notably, the liquid sampling atmospheric pressure glow discharge (LS-APGD) ionization stands out as an innovative technique for combined atomic and molecular analysis [24, 25]. A liquid sample is directly introduced into a micro-discharge; i.e., a low-pressure gas undergoes ionization to form a plasma, which ionizes the analytes in the sample microdroplets. The complete droplet consumption makes it ideal for quantitation. Its rapidity makes it efficient for various applications without requiring extensive sample preparation. LS-APGD has been proven capable of ionizing analytes from elemental species to low-polarity polycyclic aromatic hydrocarbon compounds [8, 26]. However, the formation of adduct or fragment ions during ionization could complicate the interpretation of mass spectra with insufficient resolution, leading to potential false identifications or difficulty distinguishing closely related compounds. These types of challenges can be overcome by HRMS that offers enhanced selectivity and improves the identification and quantification of specific analytes in complex matrices. The HRMS performance can be provided by Orbitrap Fourier transform mass spectrometry (FTMS) with absorption mode FT strategies [27–29].

In FTMS, both the ion's identity and quantity are encoded within time-domain signals, termed "transients" [30]. Mass spectra emerge from Fourier transformation (FT) of the transients, by suitable calibration strategies. Contemporary FTMS resorts on three alternative modes for signal processing [30, 31]:

(a) magnitude FT (mFT), in which the amplitude modulus (absolute value of a complex number) distributions are captured and for which an incoherent superposition summation is done. The mFT spectral representation suffers from limitations in resolution and sensitivity (mass spectra contain only positive data points, limiting the mean of noise value upon spectral averaging).
(b) absorption FT (aFT), in which the amplitude and phase distributions are captured, as a coherent summation. The aFT spectral representation is data intensive and prone to artifacts, e.g. when the ion initial phase is not interscan stable, but offers the benefits of higher resolution (doubling the mFT performance) and sensitivity (both negative and positive data points are present in mass spectra, offering a mean of noise close to zero upon spectral averaging).
(c) enhanced FT (eFT), which is a more recent compromise between the former two: the aFT peak resolution and mFT baseline (only positive data points) [31].

The eFT mass spectra were introduced exclusively for the Orbitrap models, starting with the LTQ Orbitrap Elite™ [32]. Predecessor models, including the LTQ Orbitrap XL™ [33], which is the platform of this study, were restricted to producing mFT mass spectra. Thus, equipping the LTQ Orbitrap XL with the aFT mass spectra representation capability is desirable. Notably, the data are contained in the aFT mass spectra mirrors found in the transients. Conversely, the information content in mFT and eFT mass spectra experiences reduction when compared to aFT.

Recent developments have shown that, when provided with transients for post-processing, it is possible to generate aFT mass spectra by phasing the ion signals for two primary FTMS instruments: Orbitraps and ion cyclotron resonance (ICR) [34–37]. These software-driven approaches have been enhanced and streamlined by introducing in-hardware phased transient acquisition using external high-performance data acquisition and processing (DAQ/P) systems [29, 38, 39]. Utilizing these systems for transient acquisition offers several benefits over the traditional method of transient detection and processing in FTMS, as described for different Orbitrap and ICR models [40–44]. However, achieving the desired aFT performance with the mFT-only LTQ Orbitrap XL instrument may appear unrealistic due to the anticipated variations in the initial ion phases and potential inaccuracies in triggering signals in this generation of Orbitrap instruments.

Here, we detail the first successful integration of an external high-performance DAQ/P system with the continuous

beam ion source LTQ Orbitrap XL, facilitating access to the aFT mass spectra. The enhancement, in conjunction with the LS-APGD ion source, elevates this Orbitrap's analytical performance, addressing the inherent challenges of CP analysis.

Experimental methods

Materials and chemicals

Solvent and blank were HPLC-grade methanol (Sigma-Aldrich, Schnelldorf, Germany) and Milli-Q water (conductivity 0.056 µS cm^{-1}, Millipore Milli-Q, Serv-A-Pure, Bay City, USA) in a 70:30 mixture. To calibrate the instrument and investigate the mass accuracy of the set-up, Pierce™ LTQ Velos ESI positive and negative ion calibration solutions (product numbers, respectively: 88323, 88324) from Thermo Fisher Scientific (Langerwehe, Germany) were used. The calibration mixture contained caffeine (200 µg), MRFA (10 µg), and ultramark 1621 (0.001% v/v) in a solution of acetonitrile/methanol/water/acetic acid (50/25/24/1) per 10 mL of solution. The single-chained C_{18} CP were synthesized as described previously [23, 45]. The CP were stored in a 500 ng/µL stock concentration in a methanol–water (1:1) mixture. Diluted samples were generated from the stock solutions ranging from 1 to 8 ng/µL.

Plasma ion source

The licensed (Pacific Northwest National Laboratory, Richland, WA, USA) LS-APGD ion source was described elsewhere [26, 46]. The LS-APGD was mounted in place of the original ESI source via a custom interface. The LS-APGD configuration features a solution electrode that acts as the cathode, and a 90° positioned stainless-steel counter electrode serving as the anode with a positive potential. A microplasma is lit on the liquid surface, ionizing the sample molecules, with the resultant ions channeled into the MS via the ion transfer capillary. Analyte solutions were directly introduced into the LS-APGD microplasma using a 5-mL Luer Lock syringe (Fusion 100, Chemyx, Stafford, TX, USA). A sheath gas flow of He (99.99%, Pangas, Switzerland) is introduced through the stainless-steel capillary of the anode. The solution ground cathode that delivers the analyte is made out of an outer hollow stainless-steel capillary (316 SS, 1.6 mm outer diameter, 0.8 mm inner diameter, McMaster-Carr, Elmhurst, IL, USA) and an inner capillary made of fused silica (inner diameter 250 µm, outer diameter 360 µm, Molex, Lisle, IL, USA). Experimental parameters of the LS-APGD, such as gas flow rate, liquid flow rate, and discharge current, are controlled using a custom-made control box (GAA Custom Electronics, Kennewick, WA, USA). The following LS-APGD conditions were used for all experiments in this work: helium sheath gas flow rate was 500 mL/min, liquid flow rate with the analyte 30 µL/min, discharge current 30 mA (0–1 kV, 10 kΩ), sampling distance 1.0 mm, and an electrode gap of 0.8 mm.

Mass spectrometer

The mass spectra were acquired using an LTQ Orbitrap XL mass spectrometer (Thermo Fisher Scientific, Bremen, Germany) hyphenated with an LS-APGD ion source. The LTQ Orbitrap XL instrument was calibrated in both positive and negative ion modes using Pierce™ LTQ Velos ESI calibration solutions using the conventional ESI ion source. The LS-APGD Orbitrap experiments were run in the negative polarity to analyze the CP in a mass range *m*/*z* 200–1500 at the resolution settings 30,000 and 100,000 at *m*/*z* 400 (separate experiments). The corresponding transient lengths are 384 ms and 1536 ms (mFT spectral representation). The automatic gain control (AGC) target was set to 10^4 or 10^6. The ion injection (accumulation) times were optimized regarding the AGC target values. The investigated injection times were 100 ms, 250 ms, 500 ms, 750 ms, and 1000 ms. The Orbitrap was operated via a standard in-built DAQ system and instrument control software (Xcalibur, Thermo Fisher Scientific).

External data acquisition and processing system

The LTQ Orbitrap XL instrument was externally interfaced with a high-performance data acquisition and processing (DAQ/P) system (FTMS Booster X2, Spectroswiss, Lausanne, Switzerland), Figure S1, Supporting Information. Previously, similar DAQ/P systems were interfaced with the more recent Q Exactive Orbitraps [29, 38, 43]. There are principal differences in the construction of the prior generation, LTQ Orbitrap XL, and the newer generation, Q Exactive, instruments. The prior generation instruments were designed to exclusively deliver the mFT mass spectra. In addition, the initial period in their transient subject to perturbations in the switching of the high-voltage electronics was substantially longer than in the newer generation instruments—on the order of ms. The latter is a disadvantage for properly phasing the ion signals in the transients as the point of phase coherence for all ions in the mass analyzer is thus further away. Finally, the quality of the triggering signals (e.g., trigger signal rise time and timing) in the prior generation Orbitraps is not as accurate as in the newer generation instruments. These triggering signals are input to the DAQ/P system, at the time ions are ejected from the C-trap, on their way to the Orbitrap mass analyzer [47].

It is thus logical that the generation of the in-hardware phased transients and aFT mass spectra was first reported for the newer Orbitraps. However, in this work, we have

successfully addressed the problems of the prior generation Orbitraps and enabled the generation of the in-hardware phased transients and the corresponding aFT mass spectra. To do so, we employed two triggering signals to form sufficient quality start and stop triggers, instead of a single triggering signal that is sufficient for the newer generation Orbitraps. The firmware of the FTMS Booster X2, including the Xilinx and LabVIEW programming of the on-board field-programmable gate array (FPGA) chip for the in-line digital signal processing, has been developed to match the signal quality and triggering logic of the LTQ Orbitrap XL.

Ion signals generated with the induced ion current detection system of the Orbitrap mass spectrometer are first differentially amplified with the original pre-amplifier located near the mass analyzer (Figure S1). After the pre-amplifier, the ion signals as analog transients are sampled (digitized) with a conventional original manufacturer's in-built DAQ system and yield mass spectra in the magnitude mode FT (.RAW mass spectra). In parallel, a minor part of the analog ion signals is taken after the pre-amplifier and sent to the external high-performance DAQ/P system (FTMS Booster X2). As the time-domain ion signals enter the DAQ/P system, they are first amplified with the user-defined amplification gains using the custom-built amplifier (Spectroswiss). The amplified ion signals are digitized with a digitization (sampling) frequency of around 250 MHz on a 14-bit digitizer (National Instruments, Austin, TX, USA). The digitized ion signals are first processed with the real-time digital signal processing on the embedded FPGA chip. Then, the pre-processed data is rapidly transferred by the high-speed chassis (National Instruments) to be further processed on the central processing unit (CPU) of the onboard controller (National Instruments).

The transients, recorded with the FTMS Booster X2, were converted into aFT mass spectra using Peak-by-Peak Base Edition software (version 2023.4.1, Spectroswiss). In addition, FTMS data, including transients, isotopic envelopes, and broadband mass spectra, for the organic compounds of interest, were simulated using a dedicated software tool, FTMS Simulator (Spectroswiss) [30]. The latter tool was used to perform in silico transient generation for the parameters specific to ion detection with an LTQ Orbitrap XL instrument.

Results and discussion

Experimental set-up characterization: calibration mixture analysis

The experimental set-up comprises three primary components, interfaced together for the first time: (i) an LS-APGD ion source, (ii) an LTQ Orbitrap XL mass spectrometer, and (iii) a high-performance DAQ/P system (Figure S1). The experimental set-up underwent an initial characterization and assessment using a standard calibration mixture widely employed in Orbitrap FTMS. The LS-APGD ion source efficiently produced protonated species of the calibrants across a broad mass range. A single-scan mass spectrum of this mixture, performed in positive ion mode, displayed the expected ion signals from caffeine, the MRFA peptide, and ultramark (Fig. 1).

Additionally, the data show that a 409-ms transient signal was successfully recorded using the external high-performance DAQ/P system. This duration slightly surpasses the anticipated transient length of 384 ms, based on a resolving power setting of $R = 30{,}000$ at m/z 400, by a 25-ms overhead. Notably, the 409-ms transient period was not directly selected by the user, but is a result of a user-selected resolution setting that required a 384-ms transient and the allied Orbitrap system overhead of 25 ms. Using the FTMS Booster X2 system, a single-scan transient enabled the direct generation of an absorption FT (aFT) mass spectrum employing half-window apodization, with no discernible peak shape anomalies (Fig. 1, insets). As expected, the aFT peak resolution doubles that of the initial mFT spectral output. A single-scan mass spectrum reveals a remarkable spectral dynamic range (DR) spanning 3.5 orders of magnitude. Furthermore, some low-abundance peaks appear solely in the aFT mass spectrum and are absent in the mFT data (Fig. 1, insets). This difference might be attributed to the characteristics of the DAQ systems used, rather than a diminished profile representation in the mFT mass spectrum, considering that it is based on single-scan data. Therefore, the external high-performance DAQ/P system has showcased its potential to capture in-hardware phased transients, even with the initial generation LTQ Orbitrap instruments.

In FTMS, averaging multiple transients or mass spectra is crucial for enhancing data statistics [29]. The projected analysis of CP-containing samples is performed via direct infusion using the LS-APGD ion source and requires averaging numerous single-scan mass spectra or transients. Such data averaging can be vulnerable to scan-to-scan frequency shifts, leading to cumulative data artifacts, which may manifest as a drop in resolution or split peaks. The employed experimental configuration demonstrates remarkable interscan frequency stability, as is evidenced by the ability to average multiple (100) transients without compromising resolution or peak shape quality, as depicted in the aFT mass spectrum (Figure S2, Supporting Information).

Moreover, the averaged data unveils an expansion in the spectral dynamic range reaching five orders of magnitude (Figure S2, insets). This significant performance enhancement is attributed to the averaging of unreduced data, whether transients or full-profile aFT mass spectra, both of which yield comparable outcomes. When mFT mass spectra are averaged

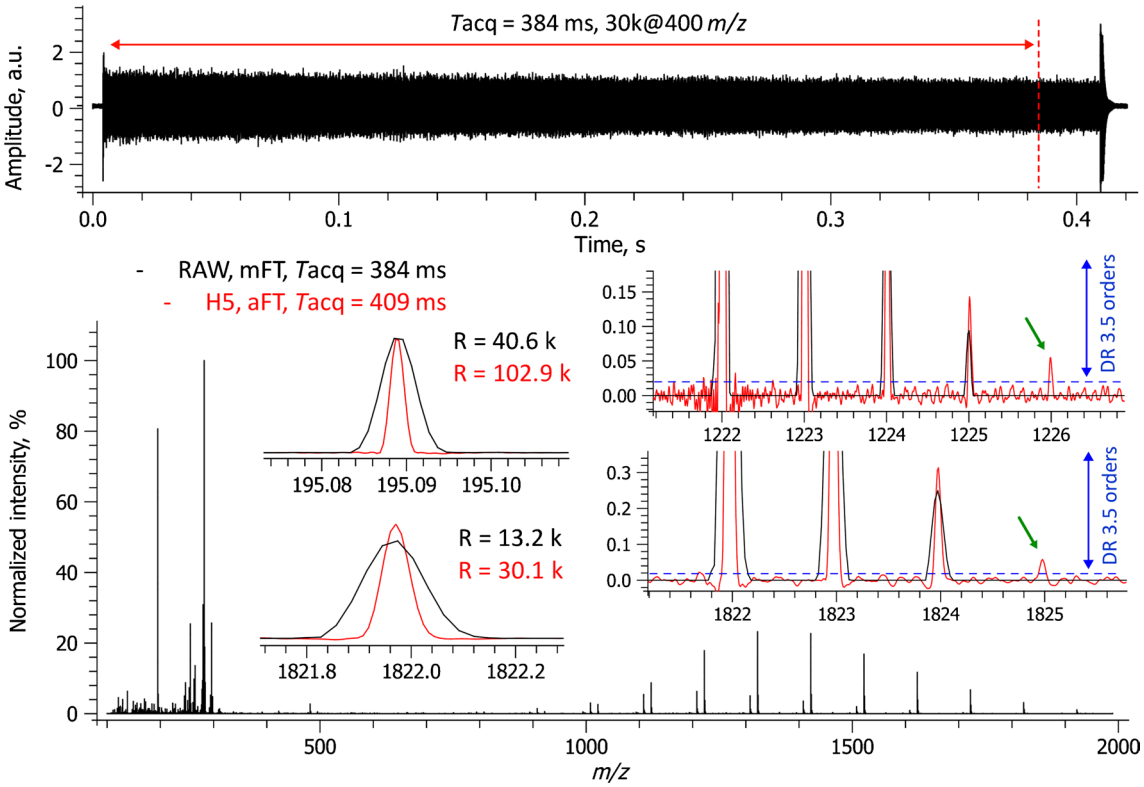

Fig. 1 Calibration mixture analysis in a positive ion mode with an LTQ Orbitrap XL equipped with a glow discharge ion source and a high-performance DAQ/P system. A single-scan mass spectrum is shown (positive ion polarity, resolution setting 30,000 at *m/z* 400, AGC 2e6, ITmax 200 ms). The resolution increase between the mFT (.RAW, reduced profile) and aFT (.H5, full profile) mass spectra is as expected and confirms the high performance of the external DAQ/P system. An excellent spectral dynamic range of 3.5 orders of magnitude is shown for a single scan

in full or reduced profile mode, the resultant increase in the spectral dynamic range is less stark [29, 48]. This distinction is further emphasized when comparing aFT and mFT mass spectra (Fig. 2, insets).

An analysis using the calibration mixture in the negative ion mode was carried out to assess further the developed experimental set-up's aptitude for analyzing CP-containing samples. The results validate the high performance of the set-up in the negative ion mode, including an expected increase in resolution by a factor of 2 in the aFT mode when compared to the mFT mode and an overhead of circa 26 ms between the transients (data not shown). The overheads observed in the negative ion mode (26 ms) align with those noted in the positive ion mode (25 ms), and other performance improvements, shown in Fig. 1. In summary, the data derived from the calibration mixture indicate the platform's potential suitability for CP analysis.

Polychlorinated paraffin sample analysis: CP, CO, and CdiO compounds

Following the platform benchmarking described above, the LS-APGD Orbitrap FTMS equipped with the high-performance DAQ/P system was evaluated for the analysis of CP-containing samples. A single-chain C18-CP material of medium chlorination degree was analyzed using the ESI and LS-APGD LTQ Orbitrap XL FTMS and compared with data published earlier, using the APCI time-of-flight (TOF) MS [23]. The APCI TOF MS data revealed presence of seven CP homologs, from Cl_4 to Cl_{10} (Table 1). The ESI LTQ Orbitrap XL FTMS analysis resulted in a similar CP-like distribution formed by the $[M+Cl]^-$ adducts (data not shown). A detailed analysis of the CP-containing samples performed with the LS-APGD LTQ Orbitrap XL FTMS at $R = 30{,}000$ resolution setting is shown in Fig. 2.

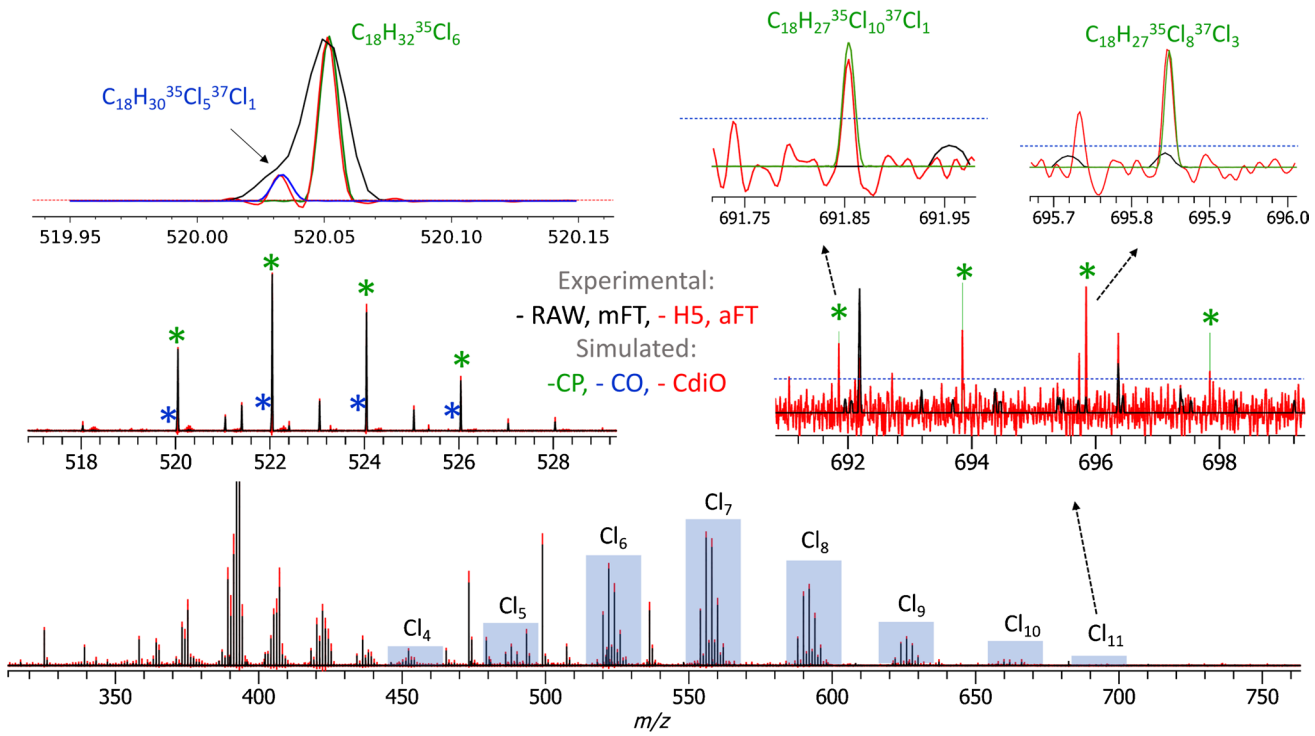

Fig. 2 Polychlorinated compound analysis with an LTQ Orbitrap XL equipped with a glow discharge ion source and a high-performance DAQ/P system. Results of averaging of 100 transients are shown (negative ion polarity, resolution setting 30,000 at *m/z* 400, AGC 1e6, ITmax 200 ms). Mass spectra representation in the aFT mode (.H5, full profile, shown in red) resolves doublets that remain unresolved in the mFT mode (.RAW, reduced profile, shown in black) spectral representation. The identified compound classes are the chlorinated paraffins (CP, simulated peaks are shown in green) and chlorinated olefins (COs, simulated peaks are shown in blue), detected as nitrate anions, $[M+NO_3]^-$

Table 1 Elemental compositions and monoisotopic masses of neutral and charged C_{18}-CP species with a general formula $C_nH_{2n+2-x}Cl_x$, $n=18$. The reference values are calculated using the FTMS data simulations (FTMS Simulator, Spectroswiss)

Chlorination degree	Molecule	M monoisotopic neutral, Da	M monoisotopic $[M+Cl]^-$, *m/z*	M monoisotopic $[M+NO_3]^-$, *m/z*
4	$C_{18}H_{34}Cl_4$	390.1414	425.1109	452.1298
5	$C_{18}H_{33}Cl_5$	424.1024	459.0719	486.0908
6	$C_{18}H_{32}Cl_6$	458.0635	493.0329	520.0519
7	$C_{18}H_{31}Cl_7$	492.0245	526.9939	554.0129
8	$C_{18}H_{30}Cl_8$	525.9856	560.9550	587.9739
9	$C_{18}H_{29}Cl_9$	559.9466	594.9160	621.9350
10	$C_{18}H_{28}Cl_{10}$	593.9076	628.8770	655.8960
11	$C_{18}H_{27}Cl_{11}$	627.8686	662.8380	689.8570

The soft ionization conditions in the LS-APGD MS supported the preferential formation of nitrate-adduct $[M+NO_3]^-$ ions (Fig. 2 and Table 1). Therefore, the following study focused on the analysis of the $[M+NO_3]^-$ ions. The presence of nitric acid or nitrate salts has previously been reported to produce nitrate-adduct ions under ESI conditions [49]. As none of those was present in the sample, it is likely that the NO_3^- can be generated either by electron ionization or by charge transfer from the ionized plasma gas [50–52]. The presence of the NO_3^- compounds is supported by comparing the experimental and simulated data (Figure S3, Supporting Information).

The expected resolution benefits of the aFT mass spectra representation (visualized in Fig. 2, top left inset) are complemented by the increase in the S/N of the low-abundant components (visualized in Fig. 2, top right inset). Due to the data averaging of 100 scans, the abundance of the aFT peaks significantly exceeds that of the mFT ones. As a result, a series of CP containing from 4 to 11 chlorine atoms can be detected. For example, even the very low abundance Cl_{11}

group of C_{18}-CP components, such as $C_{18}H_{27}{}^{35}Cl_{10}{}^{37}Cl_1$ and $C_{18}H_{27}{}^{35}Cl_8{}^{37}Cl_3$, can be detected and assigned (Fig. 2, top right inset). Notably, it was not reported in the original study with APCI TOF MS [23]. Moreover, due to the increase in resolution and sensitivity, an additional class of compounds, the CO, can be now resolved. The CP and CO mass spectra strongly interfere, and it is crucial in the CP analysis to separate the two. Therefore, since new techniques in the CP analysis are now shifting to longer CP, the relevance of the identification of CO and CdiO is increasing. As an example, a CP compound $C_{18}H_{32}{}^{35}Cl_6$ is now distinguished from a CO compound $C_{18}H_{30}{}^{35}Cl_5{}^{37}Cl_1$ (Fig. 2, top left inset). The accurately simulated profiles of the peaks corresponding to CP and CO components are added to the mass spectra to facilitate the visualization of the results.

The increase to $R = 100{,}000$ at m/z 400 generated the original Orbitrap transient of 1536 ms and the in-hardware phased transient (H5) of ca. 1570 ms (an expected ~30 ms overhead), which translated into the corresponding increases in selectivity and sensitivity in comparison with the $R = 30{,}000$ measurements (Fig. 3). Similar to the results reported above (Fig. 2), data averaging of the unreduced aFT mass spectra (or transients) allowed to significantly enhance S/N values for the low-abundance compounds. For example, the detection of the Cl_{10} group of CP compounds $C_{18}H_{28}{}^{35}Cl_9{}^{37}Cl_1$ and $C_{18}H_{28}{}^{35}Cl_6{}^{37}Cl_4$ is shown in Fig. 3, top right inset.

Moreover, further increased resolution and sensitivity performance enabled the detection of another class of compounds—CdiO. Figure 3, top left inset, exemplifies the detection of the corresponding Cl_6 group CdiO compound $C_{18}H_{28}{}^{35}Cl_4{}^{37}Cl_2$ in addition to the CP and CO compounds, $C_{18}H_{32}{}^{35}Cl_6$ and $C_{18}H_{30}{}^{35}Cl_5{}^{37}Cl_1$, respectively. The latter two compounds were identified at the 30,000 resolution setting (Fig. 2), but not the CdiO compound.

Figure 4 presents further evidence for the detection of all three classes—CP, CO, and CdiO—in the analysis of the CP-containing samples. The original mFT mass spectra (Fig. 4a) do not provide sufficient sensitivity and spectral dynamic range to detect the CdiO compounds, whereas the aFT mass spectra delivered by the experimental set-up in this work (Fig. 4b) enable their detection. The simulated peak profiles of the corresponding compounds are added to the experimental mass spectra to highlight the expected position and peak shape of the peaks of interest.

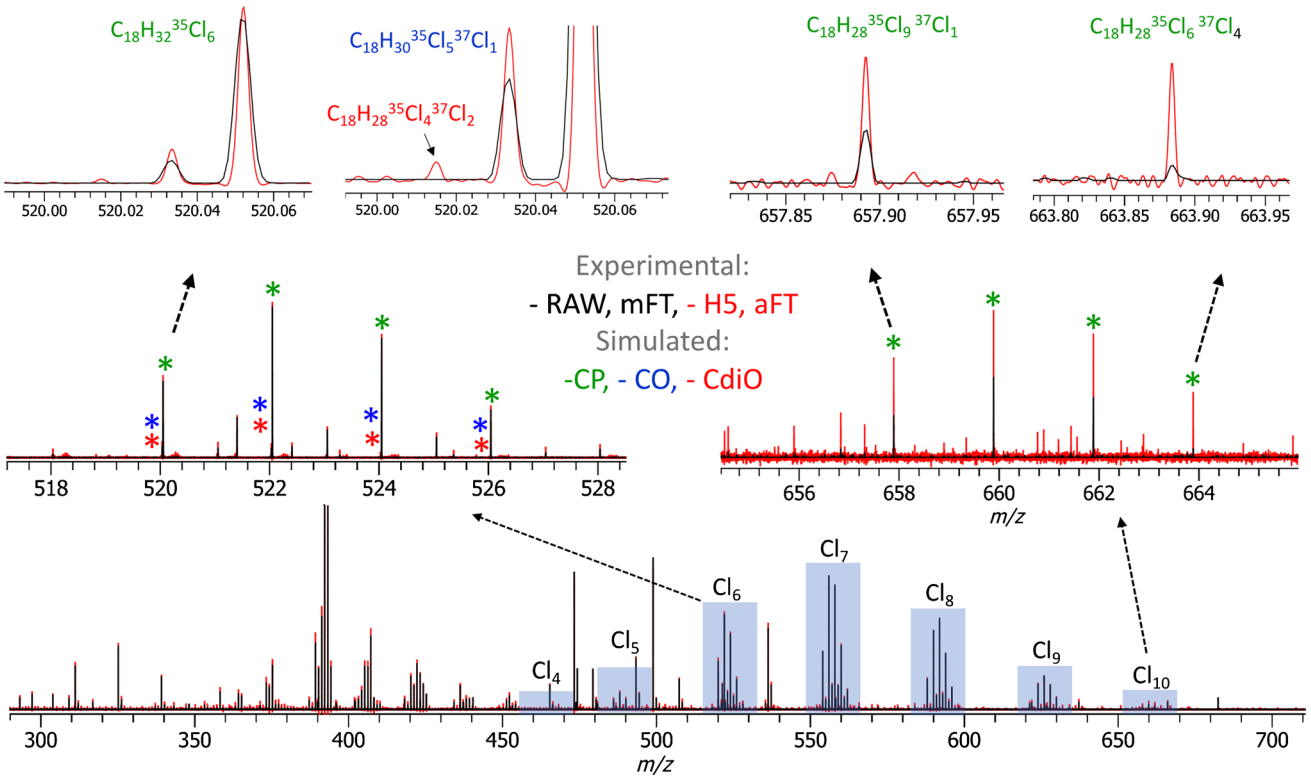

Fig. 3 Polychlorinated compounds analysis with an LTQ Orbitrap XL equipped with a glow discharge ion source and a high-performance DAQ/P system. Results of averaging of 100 transients are shown (negative ion polarity, resolution setting 100,000 at m/z 400, AGC 1e6, ITmax 200 ms). Mass spectra in the aFT mode (.H5, full profile, shown in red) show identified triplets that remain unidentified in the mFT mode (.RAW, reduced profile, shown in black) spectral representation. The identified compound classes are the chlorinated paraffins (CP, shown in green), chlorinated olefins (COs, shown in blue), and chlorinated di-olefins (CdiOs, shown in red) detected as nitrate ions, $[M+NO_3]^-$

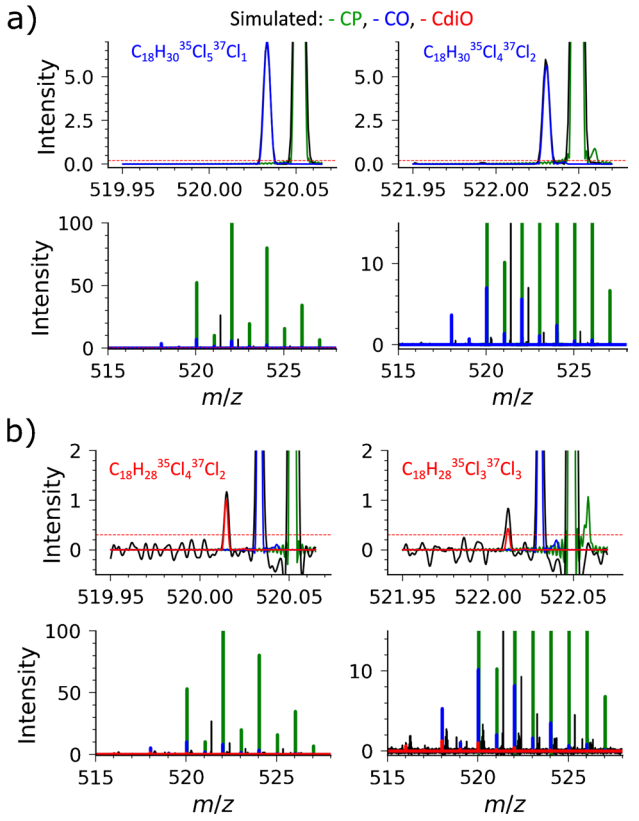

Fig. 4 Identification of CP, CO, and CdiO components in the mass spectra as presented in Fig. 3. The Cl_6 constituents of the CP and CO classes can be identified in the original mFT mass spectra (RAW) (**a**) and in the aFT mass spectra (H5). The corresponding CdiO compounds are detected only in the more sensitive mass spectra (H5, aFT) (**b**). Here, the experimental data are shown in black and simulated: CP—green, CO—blue, and CdiO—red. Experimental data and simulated isotopic envelopes normalized on the highest isotopologue

Polychlorinated paraffin sample analysis: intensity error analysis

Accuracy and precision with which peak intensities are described in the mass spectra are essential for appropriate sample analysis, including quantitation and isotopic ratio analysis. Figures 2, 3, and 4 already imply that the aFT mass spectra provide higher intensities for the low-abundant components compared to the mFT data. We performed intensity error analysis for the mass spectra presented above to quantify these differences.

The intensity error analysis method is briefly described below. First, the elemental compositions of the CP were used as the entries for the accurate simulation of the corresponding peak profiles using the FTMS Simulator tool [30]. The thus obtained simulated data were compared with the experimental peak profiles (Figure S4, Supporting Information). Intensity errors were obtained for each isotopologue in the CP distribution, and isotopic-envelope-wide intensity errors were averaged to yield the final average intensity errors (Fig. S4c, f, and Tables S1 and S2, Supporting Information). The mass accuracy values reported in Tables S1 and S2 correspond to the original external mass scale calibration of the RAW mass spectra. The aFT mass spectra calibration was performed using the same calibration coefficients and equations, demonstrating comparable mass accuracies.

The intensity errors were thus calculated for all CP detected in Figs. 2 and 3 and plotted against the number of chlorines and S/N values for the 30,000 and 100,000 resolution cases (Figs. 5 and 6), correspondingly.

Mass spectra represented in both mFT (shown in gray) and aFT (shown in red) modes are compared. The aFT results demonstrate a significant reduction in intensity errors and a higher number of identified species, particularly for the low-abundant

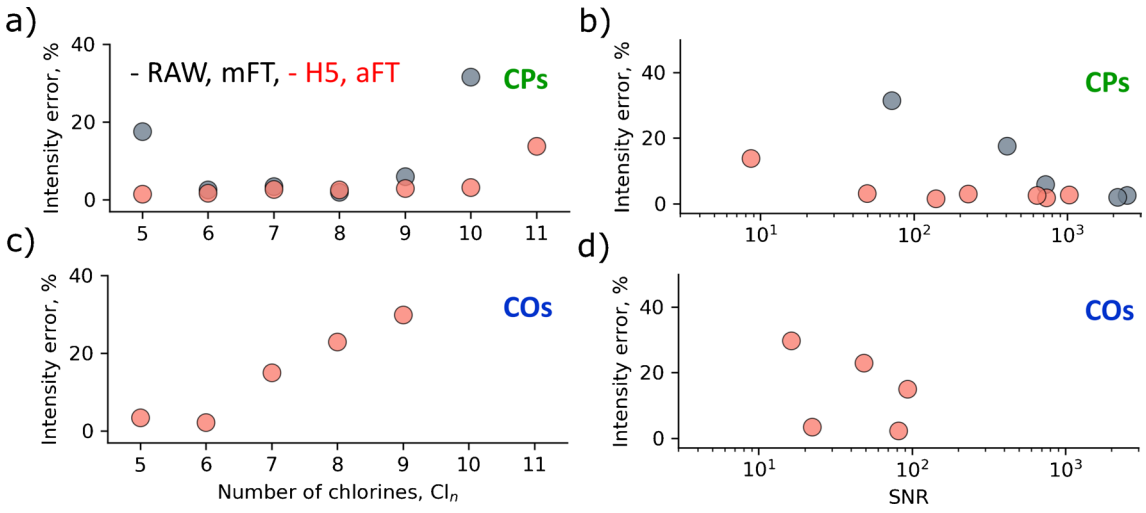

Fig. 5 Intensity error distributions for the experimental data as shown in Fig. 2 ($R = 30{,}000$) as a function of the number of chlorines (**a**, **c**) and signal-to-noise ratio (S/N) (**b**, **d**). The intensity error calculation approach is discussed in Figure S4. **a**, **b** Results for the CP, and **c**, **d** for the CO

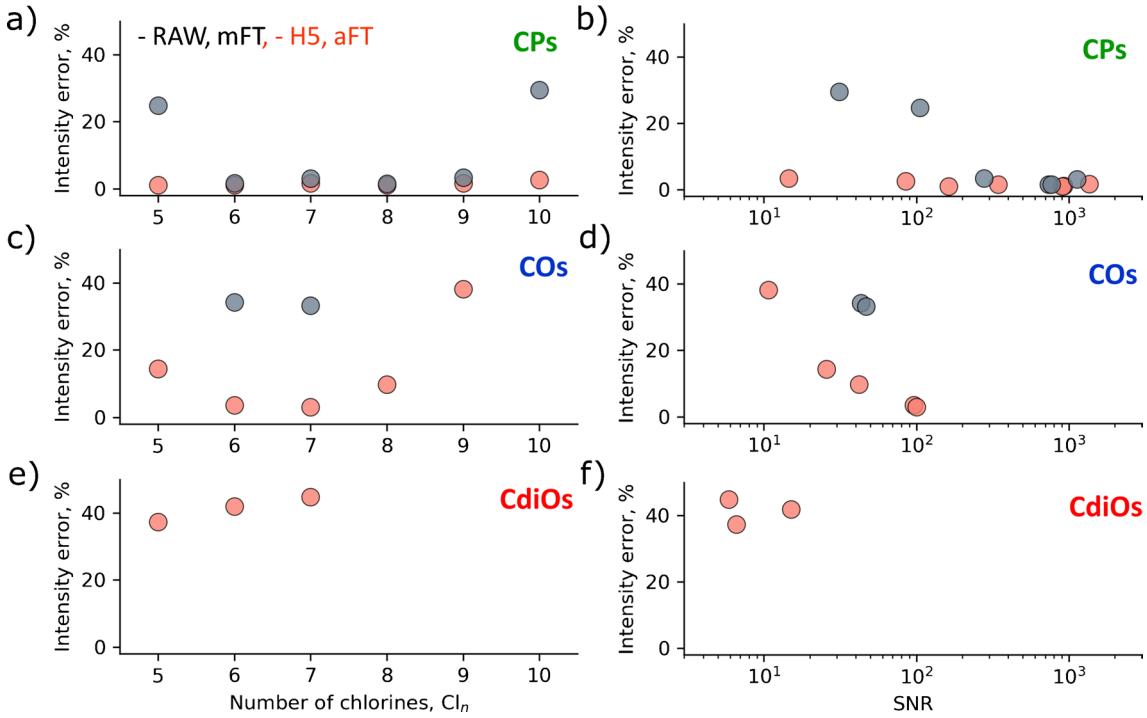

Fig. 6 Intensity error distributions for the experimental data as shown in Fig. 3 ($R = 100{,}000$) as a function of the number of chlorines (**a**, **c**, **e**) and signal-to-noise ratio (S/N) (**b**, **d**, **f**). The intensity error calculation approach is discussed in Figure S4. **a**, **b** Results for the CP; **c**, **d** for the CO; and **e**, **f** for the CdiO

Cl_n groups. CP compounds by an order of magnitude dominate CO species, which, in turn, are about an order of magnitude more abundant than the CdiO species.

Conclusions

Hyphenation between the LS-APGD ionization source and the LTQ Orbitrap XL mass spectrometer, connected in parallel to a high-performance DAQ/P system, enhanced the depth of CP complex mixture characterization. The versatility of LS-APGD, as a soft ionization technique, has been demonstrated. The LS-APGD showed an ability to generate CP-nitrate-adduct $[M+NO_3]^-$ ions. The unique feature of the DAQ/P hardware and firmware is its capacity for in-hardware-phased transient acquisition. This allowed for the aFT mass spectra representation even with the mFT-only foundational Orbitrap model. Equipped with this advanced aFT technology, our experimental set-up amplified resolution, sensitivity, and spectral dynamic range. This resulted in the successful resolution of interferences between CP, chlorinated olefins (COs), and chlorinated di-olefins (CdiOs)—three separate compound classes typically present in complex CP mixtures—at different degrees of chlorination. Furthermore, the aFT data demonstrated its superior performance to the original mFT data also in reporting the intensities of the mass spectral peaks, particularly the low abundant ones. Given that longer chains and increased chlorination degrees signify a surge in CP-related interferences, these findings and analytical capabilities hold significance for the evolution of analytical methods targeting analysis of complex mixtures in general and CP in particular. Further work should address analysis of CP with different numbers of carbon atoms and quantitation. The demonstrated capability of the developed system to enhance sensitivity and dynamic range by averaging results of multiple measurements (transients or aFT mass spectra) supports its further evaluation for the trace analysis.

Supplementary Information The online version contains supplementary material available at https://doi.org/10.1007/s00216-024-05450-2.

Acknowledgements The authors are grateful to Prof. K. Marcus (Clemson, USA) for the discussions and comments, and Dr. N. Heeb (Empa) for comments to the work. Dr. M. Knobloch (Empa) and Prof. Laurent Bigler (UZH) are acknowledged for past environmental analysis studies with state-of-the-art MS equipment that were functional to the present project idea. The project was seed funded with the Empa IRC call 2020, for developing advanced analytical technologies.

Author contribution C Masucci originally drafted the manuscript and performed the experimental tests. KO Nagornov and AN Kozhinov optimized the method for the acquisition of the aFT using the Spectroswiss hardware, while they were also heavily involved in the preparation of the graphics and revision of the manuscript. K Kraft executed some of the optimization tests and provided additional guidance to C Masucci. YO Tsybin and D Bleiner conceived and guided the research, and finalized the manuscript with all graphics.

Funding Open Access funding provided by Lib4RI – Library for the Research Institutes within the ETH Domain: Eawag, Empa, PSI & WSL.

Declarations

Conflict of interest KO Nagornov, AN Kozhinov, and YO Tsybin are employees of Spectroswiss, a company that develops hardware and software for FTMS data acquisition and processing used in this study. C Masucci and K Kraft were employees of Empa during most of the period of realization of this paper, while they were enrolled as PhD students at the University of Zurich, which determined no conflict of interest. D Bleiner is employed at Empa and serves as Adjunct Lecturer at the University of Zurich, which results in no conflict of interest.

References

1. Muir D, Stern G, Tomy G. Chlorinated paraffins. In: Hutzinger O, Paasivirta J (eds) Volume 3 Anthropogenic compounds Part K. Springer Berlin Heidelberg, Berlin, Heidelberg. 2000;203–236. https://doi.org/10.1007/3-540-48915-0_8.
2. Glüge J, Wang Z, Bogdal C, Scheringer M, Hungerbühler K. Global production, use, and emission volumes of short-chain chlorinated paraffins – a minimum scenario. Sci Total Environ. 2016;573:1132–46. https://doi.org/10.1016/j.scitotenv.2016.08.105.
3. U.S. Environmental Protection Agency Report. Short-chain chlorinated paraffins (SCCPs) and other chlorinated paraffins Action Plan. 2009. https://www.epa.gov/assessing-and-managing-chemicals-under-tsca/short-chain-chlorinated-paraffins-sccps-and-other.
4. Tomy GT. Analysis of chlorinated paraffins in environmental matrices: the ultimate challenge for the analytical chemist. In: Boer J (ed) Chlorinated paraffins. Springer Berlin Heidelberg, Berlin, Heidelberg. 2010:83–106. https://doi.org/10.1007/698_2009_39
5. Schrenk D, Bignami M, Bodin L, Chipman JK, del Mazo J, Grasl-Kraupp B, Hogstrand C, Hoogenboom L, Leblanc J-C, Nebbia CS, Ntzani E, Petersen A, Sand S, Schwerdtle T, Vleminckx C, Wallace H, Brüschweiler B, Leonards P, Rose M, Binaglia M, Horváth Z, Ramos Bordajandi L, Nielsen E. Risk assessment of chlorinated paraffins in feed and food. EFSA J. 2020;18(3):e05991. https://doi.org/10.2903/j.efsa.2020.5991.
6. Birtley RDN, Conning DM, Daniel JW, Ferguson DM, Longstaff E, Swan AAB. The toxicological effects of chlorinated paraffins in mammals. Toxicol Appl Pharmacol. 1980;54(3):514–25. https://doi.org/10.1016/0041-008X(80)90179-9.
7. Geiß S, Schneider M, Donnevert G, Einax JW, Lettmann N, Rey A, Lepper H, Körner B, Prey T, Hilger B, Engelke M, Strub M-P, Adrien H, Sawal G, Löffler D, Schillings T, Hussy I, Steinbichl P, Scharf S, Ruderisch A, Olmos JE, Javier Santos F, Bartolome A, Caixach J. Validation interlaboratory trial for ISO 12010: Water quality—determination of short-chain polychlorinated alkanes (SCCP) in water. Accred Qual Assur. 2012;17(1):15–25. https://doi.org/10.1007/s00769-011-0820-z.
8. Zhang LX, Marcus RK. Mass spectra of diverse organic species utilizing the liquid sampling-atmospheric pressure glow discharge (LS-APGD) microplasma ionization source. J Anal At Spectrom. 2016;31(1):145–51. https://doi.org/10.1039/C5JA00376H.
9. Krätschmer K, Cojocariu C, Schächtele A, Malisch R, Vetter W. Chlorinated paraffin analysis by gas chromatography Orbitrap high-resolution mass spectrometry: method performance, investigation of possible interferences and analysis of fish samples. J Chromatogr A. 2018;1539:53–61. https://doi.org/10.1016/j.chroma.2018.01.034.
10. Yuan B, Muir D, MacLeod M. Methods for trace analysis of short-, medium-, and long-chain chlorinated paraffins: critical review and recommendations. Anal Chim Acta. 2019;1074:16–32. https://doi.org/10.1016/j.aca.2019.02.051.
11. Du X, Yuan B, Zhou Y, Zheng Z, Wu Y, Qiu Y, Zhao J, Yin G. Tissue-specific accumulation, sexual difference, and maternal transfer of chlorinated paraffins in black-spotted frogs. Environ Sci Technol. 2019;53(9):4739–46. https://doi.org/10.1021/acs.est.8b06350.
12. Yuan B, Vorkamp K, Roos AM, Faxneld S, Sonne C, Garbus SE, Lind Y, Eulaers I, Hellström P, Dietz R, Persson S, Bossi R, de Wit CA. Accumulation of short-, medium-, and long-chain chlorinated paraffins in marine and terrestrial animals from Scandinavia. Environ Sci Technol. 2019;53(7):3526–37. https://doi.org/10.1021/acs.est.8b06518.
13. Glüge J, Schinkel L, Hungerbühler K, Cariou R, Bogdal C. Environmental risks of medium-chain chlorinated paraffins (MCCPs): a review. Environ Sci Technol. 2018;52(12):6743–60. https://doi.org/10.1021/acs.est.7b06459.
14. Mézière M, Cariou R, Larvor F, Bichon E, Guitton Y, Marchand P, Dervilly G, Le Bizec B. Optimized characterization of short-, medium, and long-chain chlorinated paraffins in liquid chromatography-high resolution mass spectrometry. J Chromatogr A. 2020;1619:460927. https://doi.org/10.1016/j.chroma.2020.460927.
15. Yu X, McPhedran KN, Huang R. Chlorinated paraffins: a review of sample preparation, instrumental analysis, and occurrence and distribution in food samples. Environ Pollut. 2023;318:120875. https://doi.org/10.1016/j.envpol.2022.120875.
16. Castells P, Santos FJ, Galceran MT. Evaluation of three ionisation modes for the analysis of chlorinated paraffins by gas chromatography/ion-trap mass spectrometry. Rapid Commun Mass Spectrom. 2004;18(5):529–36. https://doi.org/10.1002/rcm.1366.
17. Krätschmer K, Schächtele A. Interlaboratory studies on chlorinated paraffins: evaluation of different methods for food matrices. Chemosphere. 2019;234:252–9. https://doi.org/10.1016/j.chemosphere.2019.06.022.
18. Krätschmer K, Schaechtele A, Malisch R, Vetter W. Quantification standards - the Achilles heel of chlorinated paraffin determination? Organohalogen Compd. 2019;81:344–7.
19. Zhu J, Cole RB. Formation and decompositions of chloride adduct ions, [M + Cl]−, in negative ion electrospray ionization mass spectrometry. J Am Soc Mass Spectrom. 2000;11(11):932–41. https://doi.org/10.1016/S1044-0305(00)00164-1.
20. Ayala-Cabrera JF, Galceran MT, Moyano E, Santos FJ. Chloride-attachment atmospheric pressure photoionisation for the determination of short-chain chlorinated paraffins by gas chromatography-high-resolution mass spectrometry. Anal Chim Acta. 2021;1172:338673. https://doi.org/10.1016/j.aca.2021.338673.
21. Bogdal C, Alsberg T, Diefenbacher PS, MacLeod M, Berger U. Fast quantification of chlorinated paraffins in environmental samples by direct injection high-resolution mass spectrometry with

pattern deconvolution. Anal Chem. 2015;87(5):2852–60. https://doi.org/10.1021/ac504444d.
22. van Mourik LM, Lava R, O'Brien J, Leonards PEG, de Boer J, Ricci M. The underlying challenges that arise when analysing short-chain chlorinated paraffins in environmental matrices. J Chromatogr A. 2020;1610:460550. https://doi.org/10.1016/j.chroma.2019.460550.
23. Knobloch MC, Sprengel J, Mathis F, Haag R, Kern S, Bleiner D, Vetter W, Heeb NV. Chemical synthesis and characterization of single-chain C18-chloroparaffin materials with defined degrees of chlorination. Chemosphere. 2022;291:132938. https://doi.org/10.1016/j.chemosphere.2021.132938.
24. Quarles CD, Carado AJ, Barinaga CJ, Koppenaal DW, Marcus RK. Liquid sampling–atmospheric pressure glow discharge (LS-APGD) ionization source for elemental mass spectrometry: preliminary parametric evaluation and figures of merit. Anal Bioanal Chem. 2012;402(1):261–8. https://doi.org/10.1007/s00216-011-5359-7.
25. Marcus RK, Manard BT, Quarles CD. Liquid sampling-atmospheric pressure glow discharge (LS-APGD) microplasmas for diverse spectrochemical analysis applications. J Anal At Spectrom. 2017;32(4):704–16. https://doi.org/10.1039/C7JA00008A.
26. Marcus KR, Hoegg ED, Hall KA, Williams TJ, Koppenaal DW. Combined atomic and molecular (CAM) ionization with the liquid sampling-atmospheric pressure glow discharge microplasma. Mass Spectrom Rev. 2023;42(2):652–73. https://doi.org/10.1002/mas.21720.
27. Hoegg ED, Godin S, Szpunar J, Lobinski R, Koppenaal David W, Marcus RK. Coupling of an atmospheric pressure microplasma ionization source with an Orbitrap Fusion Lumos Tribrid 1M mass analyzer for ultra-high resolution isotopic analysis of uranium. J Anal At Spectrom. 2019;34(7):1387–95. https://doi.org/10.1039/C9JA00154A.
28. Hoegg ED, Godin S, Szpunar J, Lobinski R, Koppenaal DW, Marcus RK. Ultra-high resolution elemental/isotopic mass spectrometry ($m/\Delta m > 1{,}000{,}000$): coupling of the liquid sampling-atmospheric pressure glow discharge with an Orbitrap mass spectrometer for applications in biological chemistry and environmental analysis. J Am Soc Mass Spectrom. 2019;30(7):1163–8. https://doi.org/10.1007/s13361-019-02183-w.
29. Bills JR, Nagornov KO, Kozhinov AN, Williams TJ, Tsybin YO, Marcus RK. Improved uranium isotope ratio analysis in liquid sampling–atmospheric pressure glow discharge/Orbitrap FTMS coupling through the use of an external data acquisition system. J Am Soc Mass Spectrom. 2021;32(5):1224–36. https://doi.org/10.1021/jasms.1c00051.
30. Nagornov KO, Kozhinov AN, Gasilova N, Menin L, Tsybin YO. Transient-mediated simulations of FTMS isotopic distributions and mass spectra to guide experiment design and data analysis. J Am Soc Mass Spectrom. 2020;31(9):1927–42. https://doi.org/10.1021/jasms.0c00190.
31. Lange O, Damoc E, Wieghaus A, Makarov A. Enhanced Fourier transform for Orbitrap mass spectrometry. Int J Mass Spectrom. 2014;369:16–22. https://doi.org/10.1016/j.ijms.2014.05.019.
32. Zhurov KO, Kozhinov AN, Tsybin YO. Evaluation of high-field Orbitrap Fourier transform mass spectrometer for petroleomics. Energy Fuels. 2013;27(6):2974–83. https://doi.org/10.1021/ef400203g.
33. Blake SL, Walker SH, Muddiman DC, Hinks D, Beck KR. Spectral accuracy and sulfur counting capabilities of the LTQ-FT-ICR and the LTQ-Orbitrap XL for small molecule analysis. J Am Soc Mass Spectrom. 2011;22(12):2269–75. https://doi.org/10.1007/s13361-011-0244-3.
34. Qi Y, Barrow MP, Li H, Meier JE, Van Orden SL, Thompson CJ, O'Connor PB. Absorption-mode: the next generation of Fourier transform mass spectra. Anal Chem. 2012;84(6):2923–9. https://doi.org/10.1021/ac3000122.
35. Kilgour DPA, Nagornov KO, Kozhinov AN, Zhurov KO, Tsybin YO. Producing absorption mode Fourier transform ion cyclotron resonance mass spectra with non-quadratic phase correction functions. Rapid Commun Mass Spectrom. 2015;29(11):1087–93. https://doi.org/10.1002/rcm.7200.
36. Kilgour DPA, Wills R, Qi Y, O'Connor PB. Autophaser: an algorithm for automated generation of absorption mode spectra for FT-ICR MS. Anal Chem. 2013;85(8):3903–11. https://doi.org/10.1021/ac303289c.
37. Xian F, Corilo YE, Hendrickson CL, Marshall AG. Baseline correction of absorption-mode Fourier transform ion cyclotron resonance mass spectra. Int J Mass Spectrom. 2012;325–327:67–72. https://doi.org/10.1016/j.ijms.2012.06.007.
38. Nagornov KO, Zennegg M, Kozhinov AN, Tsybin YO, Bleiner D. Trace-level persistent organic pollutant analysis with gas-chromatography Orbitrap mass spectrometry—enhanced performance by complementary acquisition and processing of time-domain data. J Am Soc Mass Spectrom. 2020;31(2):257–66. https://doi.org/10.1021/jasms.9b00032.
39. Grgic A, Nagornov KO, Kozhinov AN, Michael JA, Anthony IGM, Tsybin YO, Heeren RMA, Ellis SR. Ultrahigh-mass resolution mass spectrometry imaging with an Orbitrap externally coupled to a high-performance data acquisition system. Anal Chem. 2024;96(2):794–801. https://doi.org/10.1021/acs.analchem.3c04146.
40. Kooijman PC, Nagornov KO, Kozhinov AN, Kilgour DPA, Tsybin YO, Heeren RMA, Ellis SR. Increased throughput and ultra-high mass resolution in DESI FT-ICR MS imaging through new-generation external data acquisition system and advanced data processing approaches. Sci Rep. 2019;9(1):8. https://doi.org/10.1038/s41598-018-36957-1.
41. Vandergrift GW, Zemaitis KJ, Veličković D, Lukowski JK, Paša-Tolić L, Anderton CR, Kew W. Experimental assessment of mammalian lipidome complexity using multimodal 21 T FTICR mass spectrometry imaging. Anal Chem. 2023;95(29):10921–9. https://doi.org/10.1021/acs.analchem.3c00518.
42. Vandergrift GW, Kew W, Lukowski JK, Bhattacharjee A, Liyu AV, Shank EA, Paša-Tolić L, Prabhakaran V, Anderton CR. Imaging and direct sampling capabilities of nanospray desorption electrospray ionization with absorption-mode 21 Tesla Fourier transform ion cyclotron resonance mass spectrometry. Anal Chem. 2022;94(8):3629–36. https://doi.org/10.1021/acs.analchem.1c05216.
43. Nagornov KO, Gasilova N, Kozhinov AN, Virta P, Holm P, Menin L, Nesatyy VJ, Tsybin YO. Drug-to-antibody ratio estimation via proteoform peak integration in the analysis of antibody–oligonucleotide conjugates with Orbitrap Fourier transform mass spectrometry. Anal Chem. 2021;93(38):12930–7. https://doi.org/10.1021/acs.analchem.1c02247.
44. Deslignière E, Yin VC, Ebberink EHTM, Rolland AD, Barendregt A, Wörner TP, Nagornov KO, Kozhinov AN, Fort KL, Tsybin YO, Makarov AA, Heck AJR. Ultralong transients enhance sensitivity and resolution in Orbitrap-based single-ion mass spectrometry. Nat Methods. 2024;21(4):619–22. https://doi.org/10.1038/s41592-024-02207-8.
45. Knobloch MC, Mathis F, Diaz OM, Stalder U, Bigler L, Kern S, Bleiner D, Heeb NV. Selective and fast analysis of chlorinated paraffins in the presence of chlorinated mono-, di-, and tri-olefins with the R-based automated spectra evaluation routine (RASER). Anal Chem. 2022;94(40):13777–84. https://doi.org/10.1021/acs.analchem.2c02240.
46. Goodwin JV, Manard BT, Ticknor BW, Cable-Dunlap P, Marcus RK. Initial characterization and optimization of the liquid sampling-atmospheric pressure glow discharge ionization source

coupled to an Orbitrap mass spectrometer for the determination of plutonium. Anal Chem. 2023;95(32):12131–8. https://doi.org/10.1021/acs.analchem.3c02367.
47. Aushev T, Kozhinov AN, Tsybin YO. Least-squares fitting of time-domain signals for Fourier transform mass spectrometry. J Am Soc Mass Spectrom. 2014;25(7):1263–73. https://doi.org/10.1007/s13361-014-0888-x.
48. Srzentić K, Nagornov KO, Fornelli L, Lobas AA, Ayoub D, Kozhinov AN, Gasilova N, Menin L, Beck A, Gorshkov MV, Aizikov K, Tsybin YO. Multiplexed middle-down mass spectrometry as a method for revealing light and heavy chain connectivity in a monoclonal antibody. Anal Chem. 2018;90(21):12527–35. https://doi.org/10.1021/acs.analchem.8b02398.
49. Li F, Byers MA, Houk RS. Tandem mass spectrometry of metal nitrate negative ions produced by electrospray ionization. J Am Soc Mass Spectrom. 2003;14(6):671–9. https://doi.org/10.1016/S1044-0305(03)00210-1.
50. Gao Y, Chu F, Chen W, Wang X, Pan Y. Arc-induced nitrate reagent ion for analysis of trace explosives on surfaces using atmospheric pressure arc desorption/ionization mass spectrometry. Anal Chem. 2022;94(14):5463–8. https://doi.org/10.1021/acs.analchem.1c05650.
51. Okumura T, Attri P, Kamataki K, Yamashita N, Tsukada Y, Itagaki N, Shiratani M, Ishibashi Y, Kuchitsu K, Koga K. Detection of NO3− introduced in plasma-irradiated dry lettuce seeds using liquid chromatography-electrospray ionization quantum mass spectrometry (LC-ESI QMS). Sci Rep. 2022;12(1):12525. https://doi.org/10.1038/s41598-022-16641-1.
52. Wolf J-C, Gyr L, Mirabelli MF, Schaer M, Siegenthaler P, Zenobi R. A radical-mediated pathway for the formation of [M + H]+ in dielectric barrier discharge ionization. J Am Soc Mass Spectrom. 2016;27(9):1468–75. https://doi.org/10.1007/s13361-016-1420-2.